ACS APPLIED MATERIALS & INTERFACES

Research Article

www.acsami.org

Crystal-Orientation-Modulated Exchange Bias in Orthorhombic-$YMnO_3/La_{0.6}Sr_{0.4}MnO_3$ Multiferroic Heterostructures

Dongxing Zheng, Junlu Gong, Chao Jin, Peng Li, and Haili Bai*

Tianjin Key Laboratory of Low Dimensional Materials Physics and Preparing Technology, Institute of Advanced Materials Physics, Faculty of Science, Tianjin University, Tianjin 300072, PR China

ABSTRACT: The magnetic properties of the all-oxide multiferroic heterostructures composed of orthorhombic $YMnO_3$ (YMO) with E-type antiferromagnetic and double-exchange ferromagnetic (FM) $La_{0.6}Sr_{0.4}MnO_3$ (LSMO) were studied. An orientation-modulated exchange bias effect, which is related to the interfacial Mn−O−Mn bond angle, was discovered. Because of the large bond angle in YMO/LSMO(100) heterostructures, a strong exchange coupling at the interface is formed. This strong exchange coupling sustains an FM phase in YMO at the interface region. The FM phase with strong magnetocrystalline anisotropy contributes to the vertical shift and exchange bias effect in (100) orientation heterostructures. When LSMO (110) and (111) were layered with YMO, the Mn−O−Mn bond angle was reduced, leading to a weakened exchange coupling at the interface, and only a relatively small exchange bias at low temperatures was visible.

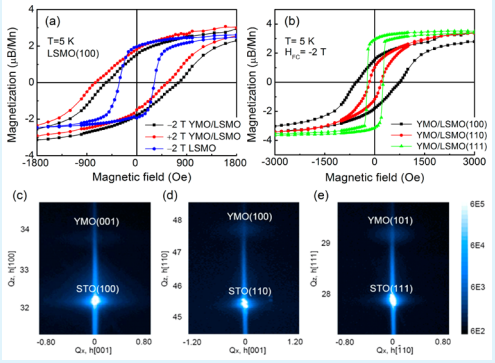

KEYWORDS: *interfacial coupling, exchange bias, multiferroic heterostructures, crystal orientation, double-exchange interaction*

INTRODUCTION

Oxide interface, a profusion field of new physics and novel functionalities, is now a key ingredient of new concepts of electronic devices. In this artificial structure, the strong correlations between charge, spin orbital, and lattice degree of freedom lead to fascinating physical properties.[1−3] The novel states appearing at the all-oxide interfaces are often completely different from those of the corresponding bulk materials. Among these artificial structures, the multiferroic-based heterostructures are particularly spectacular for the magnetic and ferroelectric orders that are integrated together, and it offers an effective route for new generation spintronic and optic−electronic devices.[4−6] So far, the exchange bias (EB), known as a result of interfacial magnetic coupling and pining effects,[7] has been used in many applications, like read heads in magnetic storage or spin valves.[8] Despite its wide use, EB is not completely understood,[8,9] especially the interfacial construction and coupling.[10] Much of the research on interfacial coupling in multiferroics-based heterostructures had emphasized that the interface reconstruction plays the key role in determining the coupling mechanism.[11] As an example, when the antiferromagnetic layers with different crystal orientations are selected, the magnetic properties of the heterostructures are completely different because there may exist compensated and uncompensated magnetic planes.[12] Furthermore, in the ferromagnetic/multiferroic systems, the interfacial construction could be modulated by an extra freedom of ferroelectric order, providing an effective way in mediating the magnetotransport properties by electric fields.[13,14]

Incorporating magnetic ordered multiferroic oxides, such as orthorhombic $YMnO_3$[15,16] (YMO) and $TbMnO_3$,[17,18] together with linear ferromagnets like $La_{0.7}Sr_{0.3}MnO_3$ and Co,[19] has drawn considerable attention recently. Multiferroic YMO, with its perovskite structure, exhibits unique and complex spin orders and belongs to the category with strong magnetoelectric coupling effect. The symmetric exchange stricition mode[20] induced polarization is not only larger than that of the others in the *o*-$RMnO_3$ systems but also makes available magnetic-field-modulated polarization, which offers new perspectives to exploit exchange coupling in multiferroic heterostructures.[21,22] In this work, we studied the EB effect in the heterostructures composed of multiferroic YMO with E-type antiferromagnetic (AFM) and double-exchange ferromagnetic (FM) $La_{0.6}Sr_{0.4}MnO_3$ (LSMO). Because both layers are manganites, a large exchange coupling can be expected because of the $Mn^{3+}−O^{2−}−Mn^{4+}$ double exchange interaction at the interface of YMO/LSMO. Moreover, by strain engineering, YMO with different crystal orientations has been fabricated on LSMO/$SrTiO_3$ substrates. Thus, completely different interface structures can be formed in those heterostructures ,and interface structure modulated EB effect was achieved.

EXPERIMENTAL DETAILS

The fabrication of YMO films is essential for devices applications as the bulk orthorhombic $RMnO_3$ samples with smaller *R* ions (*R* = Y and Ho−Lu) can only be synthesized under high oxygen pressure.[21] For the epitaxial growth of the YMO thin films with different crystal orientations, the choice of suitable substrates is the critical point. The lattice parameters of bulk YMO are *a* = 5.240 (3.706) Å, *b* = 5.797

Received: March 31, 2015
Accepted: June 17, 2015
Published: June 17, 2015

DOI: 10.1021/acsami.5b02783
ACS Appl. Mater. Interfaces 2015, 7, 14758−14762

(4.099) Å, and c = 7.361 (3.681) Å in the space group of *Pbnm*.[23] The values in the parentheses indicate those reduced to the cubic setting, namely $a/\sqrt{2}$, $b/\sqrt{2}$, and $c/\sqrt{2}$.[24] The lattice parameters meet with the $SrTiO_3$ (STO) substrate properly with the lattice misfit smaller than 6% in all orientations.

Through the lattice match of STO single substrates, the heterostructures composed of the ferromagnetic LSMO and multiferroic YMO were fabricated by radio frequency sputtering. The LSMO layer was first deposited on the STO substrate. During growth, the substrate temperature was kept at 810 °C in a mixed atmosphere with argon (50 sccm) and oxygen (30 sccm). For the fabrication of YMO layer, the growth conditions were changed to a substrate temperature of 830 °C and a mixture of argon (100 sccm) and oxygen (30 sccm). The crystal structures were analyzed by X-ray diffraction (XRD) and transmission electron microscopy (TEM), respectively. Magnetic properties were measured using a Quantum Design magnetic property measurement system (MPMS).

RESULTS AND DICUSSION

Figure 1 shows the X-ray diffraction patterns corresponding to the YMO/LSMO heterostructures deposited on (100)-, (110)-, and (111)-oriented STO. Because of the close lattice parameters of LSMO (3.880 Å) and STO (3.905 Å), their diffraction peaks coincide. No impurity phase was observed for any orientation samples. From the diffraction patterns, the out-of-plane texture is YMO(001)/LSMO(100)/STO(100), YMO(100)/LSMO(110)/STO(110), and YMO(101)/LSMO(111)/STO(111). The heteroepitaxial growth was further confirmed by examining the φ scans and tilt scans as shown in Figure 1d–f. The patterns of φ scan were obtained by keeping the Bragg angle at (112), (112), and (200) with the 2θ angle of 32.4, 32.4, and 34.3° for (001)-, (100)-, and (101)-oriented YMO, respectively. In the tilt scans, the corresponding planes for different oriented YMO were collected. Symmetric X-ray reciprocal space maps (RSM) around (100), (110), and (111) reflections for the three orientation heterostructures were collected, as shown in Figure 1g–i. In the RSM, the spots of the LSMO can hardly be seen because of the small thickness (8 nm). The spots corresponding to YMO and STO appear at virtually the same in-plane reciprocal space parameters,

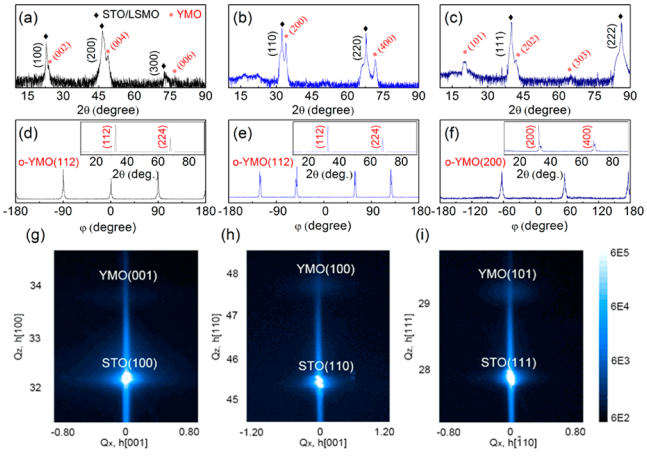

Figure 1. XRD θ–2θ patterns of the YMO/LSMO heterostructures on (a) (100)-, (b) (110)-, and (c) (111)-oriented STO. Data from φ scans of YMO (d) (112) for (002) orientation, (e) (112) for (200) orientation, and (f) (200) for (101) orientation. Insets are the corresponding tilt scans for different orientations. Symmetric RSM of YMO/LSMO heterostructures on (g) (100)-, (h) (110)-, and (i) (111)-oriented STO.

indicating that the YMO layer initially grows with the in-plane lattice parameter of the STO. These results can thus be referred to the strain-induced growth.

TEM was performed to investigate the microstructure at the YMO/LSMO interfaces. Figure 2 shows the high-resolution

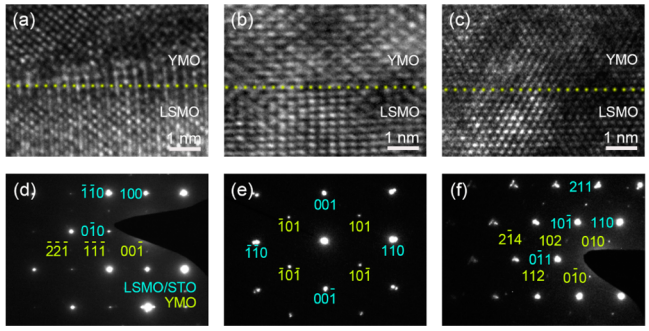

Figure 2. HRTEM images of the interface between YMO and LSMO layers on (a) (100), (b) (110), and (c) (111) STO substrates. Corresponding SAED patterns of the heterostructures on (d) (100), (e) (110), and (f) (111) STO substrates.

TEM (HRTEM) image and selected-area electron diffraction (SAED) of the YMO/LSMO heterostructures with different crystal orientations. The images clearly indicate the formation of YMO on the LSMO layer with well-defined and clear atomic interfaces. In addition, the epitaxial relationships of these heterostructures are further confirmed by the corresponding SAED patterns, as shown in Figure 2d–f. In Figure 2d, with the same situation as that in XRD caused by the close lattice parameters, the diffraction points of LSMO and STO substrates are overlapped. The crystal zone axis of LSMO and YMO is [001] and [110], respectively. Thus, the epitaxial relationship is YMO(001)[110] || LSMO(100)[001]. For the other two orientations, the epitaxial relationships are YMO(100)[010] || LSMO(110)[1̄10] and YMO(101)[010] ||LSMO(111)[1̄01,] respectively.

Figure 3a shows the typical magnetization loops of YMO(50 nm)/(100)-LSMO(12 nm) heterostructure with an in-plane magnetic field of 2 T (red) and −2 T (black) cooling from 350 to 5 K. As a comparison, the M–H loop of a single 12 nm thick LSMO layer (blue) in Figure 3a and 50 nm thick YMO layer (green) in Figure 3b are also shown. The heterostructure exhibits a clear enhancement of coercive field ($H_C \approx 660$ Oe) as compared to that of a single LSMO layer ($H_C \approx 300$ Oe) at low temperatures. Vertical and horizontal shifts occurred, and the shift directions are opposite to themselves when the cooling field is changed from 2 to −2 T. As expected from the conventional EB effect, the shift of the hysteresis loop depends on the coupling mechanism at the interface, namely, opposite to the cooling field direction for ferromagnetic coupling and in the same direction to the cooling field for antiferromagnetic coupling. In this system, the pinned and uncompensated spins at the FM and AFM layer are ferromagnetic coupling as the shift of the hysteresis loop is opposite to the direction of the cooling field.[10,25] Besides, the vertical shift of the M–H loops is also observed, which has the same sign as the cooling field shown in Figure 3b. The temperature dependence of the vertical shift is shown in Figure 3c; a shift of ~0.15 μ_B/Mn is visible at 5 K. With the increase of temperature, the shift decreases and finally disappears around 50 K. This vertical shift was also reported in Paul's work, which is induced by the

DOI: 10.1021/acsami.5b02783
ACS Appl. Mater. Interfaces 2015, 7, 14758–14762

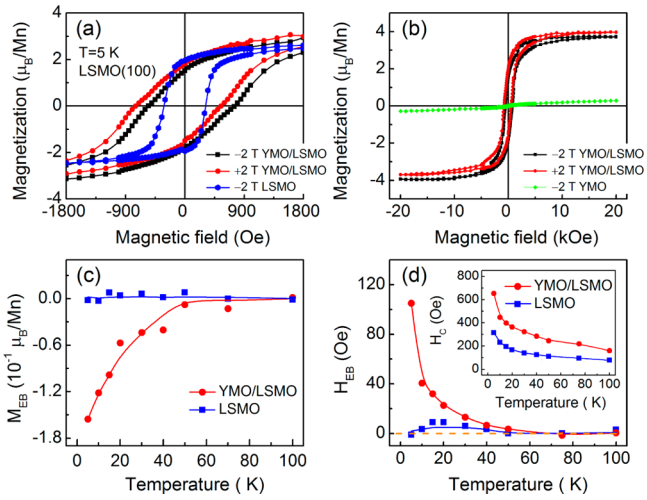

Figure 3. (a) $M-H$ loops of a YMO/(100)-LSMO heterostructure and a single LSMO layer measured along the [001] direction at 5 K after field cooling from 350 K. (b) $M-H$ loops of a YMO/(100)−LSMO heterostructure and a single YMO layer. Temperature dependence of the (c) vertical shift and (d) EB field in the YMO/LSMO heterostructure and a single LSMO layer. Inset shows the temperature dependence of coercive field.

formation of ferromagnetic phase with strong magneto-anisotropy in the YMO side at the interface.[15,16,26]

The temperature dependence of EB effect and coercive field for both the LSMO/YMO heterostructures and single LSMO layers are shown in Figure 3d. The EB effect in the heterostructures presents strong temperature-dependent behavior and disappears around 45 K, whereas almost no EB effect is visible in the LSMO single layer. This trend is consistent with the temperature dependence of vertical shift, indicating that the horizontal and vertical shifts are correlated to each other. These effects indicate that the YMO layer exhibits a strong magnetic anisotropy at low temperatures and pinned the magnetization moment of the LSMO layer.[27−29]

As mentioned above, the YMO layer plays an important role in the EB field and the enhanced coercive field in the (100) oriented heterostructure. What is the situation in heterostructures with other orientations? To further understand the roles of interfacial structure on the coupling, heterostructures with different crystal orientations were fabricated and measured under the same conditions, and the $M-H$ loops are shown in Figure 4. For all the orientations, the measured saturation magnetization of ∼3.6 μ_B/Mn is close to the theoretical value of 3.4 μ_B/Mn, but significant differences appear in the coercive and EB field. For the (100) orientation, a large H_C (660 Oe, twice of the value in the (110)- and (111)-oriented samples) is observed, reflecting the difference in the effective magnetic anisotropy. Meanwhile, an obvious EB effect can be observed in the (100)-oriented sample, whereas almost no EB effect appears in the (110) and (111) orientations.

For the interfacial coupling, the EB effect is thickness-dependent with the relation of $H_{EB} = J_{EB}/\mu_O M_F t_F$,[8] where J_{EB} is the interfacial exchange energy and t_F and M_F the thickness and saturation magnetization of the ferromagnetic layer, respectively. The heterostructures with different crystal orientations are shown in Figure 5. A clear thickness dependence of EB effect is observed in the (100)-oriented heterostructures. The EB field in the (100)-oriented heterostructures with different thicknesses decreases with the increasing temperature and

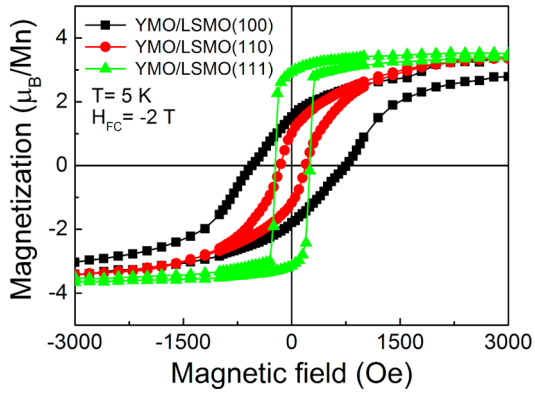

Figure 4. $M-H$ loops of YMO/LSMO heterostructures with different crystal orientations.

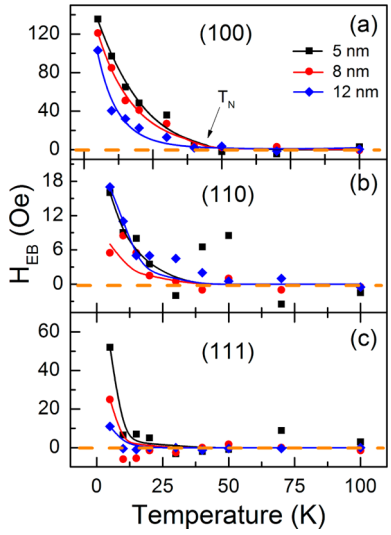

Figure 5. Temperature dependence of EB field with different LSMO thicknesses on STO (a) (100), (b) (110), and (c) (111) substrates.

disappears around the Néel temperature. The inverse dependence of the EB field with the increasing thickness in the (100)-oriented heterostructures is in good agreement with previous reports on the conventional EB system.[8] For the (110) and (111) orientations, the temperature and thickness dependence of the EB effect are quite different. The values of EB fields are much smaller than that of (100) orientation, and the disappearing temperature of EB effect is far below the Néel temperature. For the (110) orientation, the magnitude of the EB field is close to 10 Oe, which is quite small compared to the corresponding value of the (100) orientation (∼130 Oe). Although an EB field of ∼50 Oe was obtained in the (111) orientation heterostructure, it sharply decreases when the temperature increases to 10 K.

In most of the existing models, an uncompensated AFM interface is a prerequisite for the emergence of EB effect. Therefore, E-type AFM, where all the nearest-neighboring spins at the AFM/FM interface are compensated by each other, is not expected to pin the FM spins via an exchange coupling. However, it should be noted that a vertical shift of the $M-H$ loops in Figure 3b,c is indeed observed. These observations clearly indicate the formation of an FM phase of YMO side at the interface region.[15,16] To further clarify the interfacial coupling, the interface structure of the heterostructures is

DOI: 10.1021/acsami.5b02783
ACS Appl. Mater. Interfaces 2015, 7, 14758−14762

illustrated in Figure 6. We first consider the interface's atomic-stacking sequence. In (100) plane, the linear ferromagnetic

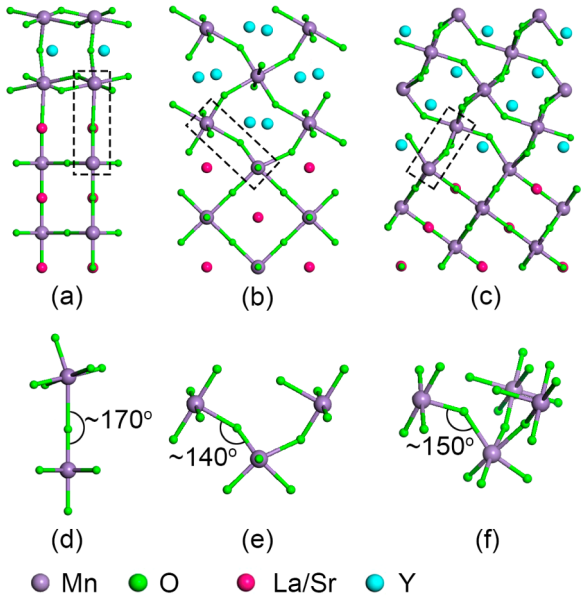

Figure 6. Illustration for the interface atomic structures of YMO/LSMO heterostructres with (a) (100), (b) (110), and (c) (111) orientations. Corresponding bond structures of $Mn^{3+}-O^{2-}-Mn^{4+}$ in (d) (100), (e) (110), and (f) (111) orientation heterostructures.

LSMO consists of stacked layers alternating between $La_{1-x}Sr_xO$ and MnO_2. YMO is composed of alternate YO and MnO_2 layers in (001) plane. Because the $La_{1-x}Sr_xO$ layer is the most stable termination with the lowest energy,[16,30,31] the possible interface is LaSrO(LSMO)−MnO_2(YMO) with the MnO_6 octahedra enclsosed in a cage with La on one side and Y on the other side, as shown in Figure 6a. In the manganese oxide system, usually there is a strong double-exchange coupling between two next-to-nearest neighbor magnetic cations through a nonmagnetic anion.[32,33] The $Mn^{3+}-O^{2-}-Mn^{4+}$ bond angle is a very important parameter for Manganite perovskites. The exchange interaction increases as the $Mn^{3+}-O^{2-}-Mn^{4+}$ bond angle approaches 180°, and the interaction is quite weak for 90°. For (100) orientation, the $Mn^{3+}-O^{2-}-Mn^{4+}$ bond angle is ∼170° so that the coupling between the LSMO and YMO layer is very strong. When the samples are cooling from 350 K with an external magnetic field, the YMO is in paramagnetic state. The moments of LSMO and YMO were pointed along the magnetic field direction. Further decreasing the temperature across the Néel temperature of YMO, the moments of YMO rearranged in AFM order. Meanwhile, the LSMO will keep the FM order. Because of the strong interaction between the $Mn^{3+}-O^{2-}-Mn^{4+}$ bonds, the Mn^{3+} moment of YMO at the interface region will preserve the FM arrangement. Moreover, the FM phase is of strong magnetocrystalline anisotropy, which contributes to the horizontal and vertical shifts of the *M*−*H* loops. Thus, the directions of the vertical and horizontal shifts are determined by the initial cooling field as shown in Figure 3b,c.

Figure 6b,c shows the interfacial atomic structures of (110) and (111) orientations, respectively. Unlike the scenario of (100) orientation, the $Mn^{3+}-O^{2-}-Mn^{4+}$ bond angles are ∼140 and ∼150° for (110) and (111) orientations, respectively, signaling the weak exchange coupling at those interfaces. Because of the weak interface exchange coupling, the EB effects of (110) and (111) orientations are only visible at low temperatures, as shown in Figure 6b,c.

CONCLUSIONS

By epitaxial strain, the YMO/LSMO heterostructures with different crystal orientations were fabricated by radio frequency sputtering. An orientation-modulated EB effect, which is related to the interfacial Mn−O−Mn bond angle, was discovered. The larger Mn−O−Mn bond angle in YMO/LSMO(100) leads to strong double-exchange interaction at the interface. This strong interfacial coupling sustains the formation of FM phase with strong magnetocrystalline anisotropy, which contributes to the vertical shift and EB effect in (100) orientation heterostructures. For the (110) and (111) orientations, the weak interfacial couplings make the EB quite small. Our results contribute to the ability to modulate the interfacial coupling by designing proper crystal structure and will facilitate the development of new generation magnetoelectric devices.

AUTHOR INFORMATION

Corresponding Author

*E-mail: baihaili@tju.edu.cn.

Author Contributions

D.Z. and H.B. designed the outline of the manuscript and wrote the main manuscript text. J.G., C.J., and P.L. contributed detailed discussions and revisions.

Notes

The authors declare no competing financial interest.

ACKNOWLEDGMENTS

H.B. was supported by National Science Foundation of China (51272174 and 11434006) and the Natural Science Foundation of Tianjin City (13JCZDJC32800).

REFERENCES

(1) Imada, M.; Fujimori, A.; Tokura, Y. Metal-Insulator Transitions. *Rev. Mod. Phys.* **1998**, *70*, 1039−1263.
(2) Hwang, H. Y.; Iwasa, Y.; Kawasaki, M.; Keimer, B.; Nagaosa, N.; Tokura, Y. Emergent Phenomena at Oxide Interfaces. *Nat. Mater.* **2012**, *11*, 103−113.
(3) Bibes, M.; Villegas, J. E.; Barthélémy, A. Ultrathin Oxide Films and Interfaces for Electronics and Spintronics. *Adv. Phys.* **2011**, *60*, 5−84.
(4) Zheng, H.; Wang, J.; Lofland, S. E.; Ma, Z.; Mohaddes-Ardabili, L.; Zhao, T.; Salamanca-Riba, L.; Shinde, S. R.; Ogale, S. B.; Bai, F.; Viehland, D.; Jia, Y.; Schlom, D. G.; Wuttig, M.; Roytburd, A.; Ramesh, R. Multiferroic $BaTiO_3$-$CoFe_2O_4$ Nanostructures. *Science* **2004**, *303*, 661−663.
(5) Chu, Y. H.; Martin, L. W.; Holcomb, M. B.; Gajek, M.; Han, S. J.; He, Q.; Balke, N.; Yang, C. H.; Lee, D.; Hu, W.; Zhan, Q.; Yang, P. L.; Fraile-Rodriguez, A.; Scholl, A.; Wang, S. X.; Ramesh, R. Electric-Field Control of Local Ferromagnetism Using a Magnetoelectric Multiferroic. *Nat. Mater.* **2008**, *7*, 478−482.
(6) Caviglia, A. D.; Gabay, M.; Gariglio, S.; Reyren, N.; Cancellieri, C.; Triscone, J. M. Tunable Rashba Spin-Orbit Interaction at Oxide Interfaces. *Phys. Rev. Lett.* **2010**, *104*, 126803.
(7) Berkowitz, A. E.; Kentaro, T. Exchange Anisotropy — A Review. *J. Magn. Magn. Mater.* **1999**, *200*, 552−570.
(8) Nogués, J.; Schuller, I. K. Exchange Bias. *J. Magn. Magn. Mater.* **1999**, *192*, 203−232.
(9) Kiwi, M. Exchange Bias Theory. *J. Magn. Magn. Mater.* **2001**, *234*, 584−595.

DOI: 10.1021/acsami.5b02783
ACS Appl. Mater. Interfaces 2015, 7, 14758−14762

(10) Malozemoff, A. P. Random-Field Model of Exchange Anisotropy at Rough Ferromagnetic-Antiferromagnetic Interfaces. *Phys. Rev. B* **1987**, *35*, 3679−3682.
(11) Cheng, Z. X.; Zhao, H. Y.; Du, Y.; Kimura, H.; Ozawa, K.; Wang, X. L. Exchange Bias in Multiferroic $BiFeO_3$ and $YMnO_3$ Multilayers: One More Parameter for Magnetoelectric Manipulation. *Scripta Mater.* **2011**, *65*, 249−252.
(12) Młynczak, E.; Matlak, B.; Kozioł-Rachwał, A.; Gurgul, J.; Spiridis, N.; Korecki, J. Fe/CoO(001) and Fe/CoO(111) Bilayers: Effect of Crystal Orientation on the Exchange Bias. *Phys. Rev. B* **2013**, *88*, 085442.
(13) Wu, S. M.; Cybart, S. A.; Yi, D.; Parker, J. M.; Ramesh, R.; Dynes, R. C. Full Electric Control of Exchange Bias. *Phys. Rev. Lett.* **2013**, *110*, 067202.
(14) Hong, X.; Yau, J. B.; Hoffman, J. D.; Ahn, C. H. Effect of Electric Field Doping on the Anisotropic Magnetoresistance in Doped Manganites. *Phys. Rev. B* **2006**, *74*, 174406.
(15) Paul, A.; Zandalazini, C.; Esquinazi, P.; Autieri, C.; Sanyal, B.; Korelis, P.; Böni, P. Structural, Electronic and Magnetic Properties of $YMnO_3/La_{0.7}Sr_{0.3}MnO_3$ Heterostructures. *J. Appl. Crystallogr.* **2014**, *47*, 1054−1064.
(16) Autieri, C.; Sanyal, B. Unusual Ferromagnetic $YMnO_3$ Phase in $YMnO_3/La_{2/3}Sr_{1/3}MnO_3$ Heterostructures. *New J. Phys.* **2014**, *16*, 113031.
(17) Tian, Y. F.; Ding, J. F.; Lin, W. N.; Chen, Z. H.; David, A.; He, M.; Hu, W. J.; Chen, L.; Wu, T. Anomalous Exchange Bias at Collinear/Noncollinear Spin Interface. *Sci. Rep.* **2013**, *3*, 1094.
(18) Tian, Y. F.; Lebedev, O. I.; Roddatis, V. V.; Lin, W. N.; Ding, J. F.; Hu, S. J.; Yan, S. S.; Wu, T. Interfacial Magnetic Coupling in Ultrathin All-Manganite $La_{0.7}Sr_{0.3}MnO_3$-$TbMnO_3$ Superlattices. *Appl. Phys. Lett.* **2014**, *104*, 152404.
(19) Barzola-Quiquia, J.; Lessig, A.; Ballestar, A.; Zandalazini, C.; Bridoux, G.; Bern, F.; Esquinazi, P. Revealing the Origin of the Vertical Hysteresis Loop Shifts in an Exchange Biased Co/$YMnO_3$ Bilayer. *J. Phys.: Condens. Matter* **2012**, *24*, 366006.
(20) Sergienko, I. A.; Dagotto, E. Role of the Dzyaloshinskii-Moriya Interaction in Multiferroic Perovskites. *Phys. Rev. B* **2006**, *73*, 094434.
(21) Ishiwata, S.; Kaneko, Y.; Tokunaga, Y.; Taguchi, Y.; Arima, T.; Tokura, Y. Perovskite Manganites Hosting Versatile Multiferroic Phases with Symmetric and Antisymmetric Exchange Strictions. *Phys. Rev. B* **2010**, *81*, 100411(R).
(22) Yu Pomjakushin, V.; Kitazawa, H.; Takayama-Muromachi, E.; Kenzelmann, M.; D Nni, A.; Harris, A. B.; Nakajima, T.; Mitsuda, S.; Tachibana, M.; Keller, L.; Mesot, J. Evidence for Large Electric Polarization from Collinear Magnetism in $TmMnO_3$. *New J. Phys.* **2009**, *11*, 043019.
(23) Muñoz, A.; Alonso, J. A.; Casais, M. T.; Martínez-Lope, M. J.; Martínez, J. L.; Fernández-Díaz, M. T. The Magnetic Structure of $YMnO_3$ Perovskite Revisited. *J. Phys.: Condens. Matter* **2002**, *14*, 3285−3294.
(24) Nakamura, M.; Tokunaga, Y.; Kawasaki, M.; Tokura, Y. Multiferroicity in an Orthorhombic $YMnO_3$ Single-Crystal Film. *Appl. Phys. Lett.* **2011**, *98*, 082902.
(25) Ohldag, H.; Scholl, A.; Nolting, F.; Arenholz, E.; Maat, S.; Young, A. T.; Carey, T. Correlation Between Exchange Bias and Pinned Interfacial Spins. *Phys. Rev. Lett.* **2003**, *91*, 017203.
(26) Zandalazini, C.; Esquinazi, P.; Bridoux, G.; Barzola-Quiquia, J.; Ohldag, H.; Arenholz, E. Uncompensated Magnetization and Exchange-Bias Field in $La_{0.7}Sr_{0.3}MnO_3/YMnO_3$ Bilayers: The Influence of the Ferromagnetic Layer. *J. Magn. Magn. Mater.* **2011**, *323*, 2892−2898.
(27) Moutis, N.; Christides, C.; Panagiotopoulos, I.; Niarchos, D. Exchange-Coupling Properties of $La_{1-x}Ca_xMnO_3$ Ferromagnetic/Antiferromagnetic Multilayers. *Phys. Rev. B* **2001**, *64*, 094429.
(28) Ding, J. F.; Wu, T.; Lebedev, O. I.; Turner, S.; Tian, Y. F.; Hu, W. J.; Seo, J. W.; Panagopoulos, C.; Prellier, W.; Van Tendeloo, G. Interfacial Spin Glass State and Exchange Bias in Manganite Bilayers with Competing Magnetic Orders. *Phys. Rev. B* **2013**, *87*, 054428.
(29) Rojas Scanchez, J. C.; Nelson-Cheeseman, B.; Granada, M.; Arenholz, E.; Steren, L. B. Exchange-Bias Effect at $La_{0.7S}Sr_{0.25}MnO_3/LaNiO_3$ Interfaces. *Phys. Rev. B* **2012**, *85*, 094427.
(30) Colizzi, G.; Filippetti, A.; Fiorentini, V. Magnetism of $La_{0.62S}Sr_{0.375}MnO_3$ Under High Pressure From First Principles. *Phys. Rev. B* **2007**, *76*, 064428.
(31) Ma, C.; Yang, Z.; Picozzi, S. Ab Initio Electronic and Magnetic Structure in $La_{0.66}Sr_{0.33}MnO_3$: Strain and Correlation Effects. *J. Phys.: Condens. Matter* **2006**, *18*, 7717−7728.
(32) Goodenough, J. B. *Magnetism and the Chemical Bond*; Interscience Publishers: New York, 1963.
(33) Kramers, H. A. L'interaction Entre les Atomes Magnétogènes dans un Cristal Paramagnétique. *Physica* **1934**, *1*, 182−192.

DOI: 10.1021/acsami.5b02783
ACS Appl. Mater. Interfaces 2015, 7, 14758−14762